

## EXPLICIT SIMULATIONS OF CONVECTIVE-SCALE TRANSPORT OF MINERAL DUST IN SEVERE CONVECTIVE WEATHER

Tetsuya Takemi \*

Dept. of Environmental Science and Technology, Tokyo Institute of Technology, Yokohama, Japan

### 1. INTRODUCTION

In the arid regions of East Asia, mineral dust emission and transport frequently occur in spring (Parungo et al. 1994) due to a high activity of mid-latitude cyclones (Qian et al. 2002). Takemi and Seino (2004a, b) investigated the relationship between dust weather development and mid-latitude cyclone activity from a statistical viewpoint and found that in the Gobi Desert the frontal activity and the embedded mesoscale cloud systems have a close tie with the dust occurrence while in the Taklamakan Desert that connection is relatively weak. With the development of an intense cyclone or a well-organized mesoscale cloud system, disastrous duststorms and dust weathers may occur over East Asia. As a case study, Takemi (1999b) and Takemi and Satomura (2000) examined the structure and dynamics of the mesoscale convective system that spawned a severe duststorm over the Gobi Desert on 5 May 1993, and showed that the duststorm was caused by a vigorous cold surface outflow which emanated from the mesoscale system. In this way, strong cyclone activity, including convective system development, is the main cause of severe duststorms, which serve as a significant source of mineral dust transport.

Meanwhile, numerical modeling studies play a crucial role in evaluating and forecasting the amount of dust emission and transport, and there are a number of numerical studies on the transport of mineral dust (e.g., Liu and Westphal 2001; Shao et al. 2002; Uno et al. 2003). A gross feature of the long-range transport of aeolian dust has been successfully simulated by these studies, and the real-time forecasting of dust transport is getting more and more feasible. However, it has also been recognized that the results of the numerical simulations significantly differ among dust models in some weather conditions. Among a number of possible reasons for the difference of the model results, the representation of vertical mixing and transport in the boundary layer and within convective-cloud updraft/downdraft is anticipated to have a significant impact on the numerical simulations.

In the present study, we will investigate numerically the effects of convective-scale updrafts and downdrafts as

well as mesoscale circulations within mesoscale convective systems on the three-dimensional (3D) transport of mineral dust by explicitly representing convective motions and cloud/precipitation development. By implementing a standard dust-emission scheme, 3D cloud-resolving simulations of a squall-line-type convective system and the associated duststorm in a severe weather setting are performed. Dynamics controlling the convective-scale dust transport is described, and thereby the processes of dust transport in convective scale as well as mesoscale are demonstrated. The case of the 5 May 1993 severe duststorm is examined here, since the basic mechanisms for the relevant mesoscale convective system were thoroughly described by Takemi and Satomura (2000). In order to focus the basic aspects of the mechanisms of convective transport processes, numerical experiments have been conducted in idealized setups with a horizontally homogeneous base state.

### 2. MODEL AND EXPERIMENTAL DESIGN

#### 2.1 Model

The numerical model used here is a non-hydrostatic cloud model, the Advanced Regional Prediction System (ARPS, Xue et al. 2000). We configured the ARPS model appropriate for our idealized simulations: we have included physics parameterizations such as Lin et al.-type cloud microphysics, Deardorff-type subgrid mixing, and surface flux calculations based on Businger et al. (1971); but we neglected the effects of the Coriolis force and radiative energy transfer.

The computational domain is 650 km in the  $x$  (east-west) direction and 120 km in the  $y$  (north-south) direction, extending from the surface to a height of 18.4 km. The base-state surface pressure is set at 850 hPa, which is taken from the observation on the 5 May 1993. The horizontal grid resolution is 2 km, and the vertical one is stretched from 20 m (at the lowest domain) up to 810 m (at the model top). Since squall lines that align in the  $y$  direction are simulated in our study, open lateral boundary conditions are specified at the  $x$  boundaries, and periodic conditions at the  $y$  boundaries.

A mineral dust emission and transport module is implemented in ARPS, and is updated at each time step of ARPS. The prognostic equation of dust mixing ratio  $q_d$  (kg

---

\*Corresponding author's address: Dr. Tetsuya Takemi, Department of Environmental Science and Technology, Tokyo Institute of Technology, G5-7, 4259 Nagatsuta, Yokohama, Kanagawa 226-8502; Email: takemi@depe.titech.ac.jp

$\text{kg}^{-1}$ ) is formulated as follows:

$$\frac{\partial}{\partial t}(\rho q_d) = F_{adv} + F_{mix} + F_{flux} + F_{grav} + F_{wet}, \quad (1)$$

where  $\rho$  is the density of air, and  $F_{adv}$ ,  $F_{mix}$ ,  $F_{flux}$ ,  $F_{grav}$ , and  $F_{wet}$  are the terms representing advection, subgrid-turbulence mixing, surface emission flux, gravitational settling, and wet scavenging, respectively.

The vertical dust flux at the surface  $F_{flux}$  is computed by an equation which defines the flux to be proportional to the fourth power of the surface friction velocity (Liu and Westphal 2001). In Liu and Westphal (2001) a parameter indicating a dust erodible fraction within each grid box is included in the flux equation; however, this study assumes that the surface is all dust erodible, and hence the fraction is set to one. The threshold friction velocity for dust emission  $u_{*t}$  is set to  $0.6 \text{ m s}^{-1}$ . We assume that the dust size is mono-distributed, and two sizes of the dust particle radius,  $1.0 \mu\text{m}$  and  $10.0 \mu\text{m}$ , are examined here (the results with the  $1\text{-}\mu\text{m}$  radius case are presented here due to the space limitation). The assumption of a mono-size distribution in this study is plausible, since the focus here is to examine the basic dynamics regarding the convective-scale transport of dust in an idealized condition. The gravitational settling is modeled in the same manner with that in Uno et al. (2003).

Wet scavenging rates of dust are diagnosed from local rain intensities with the relationship given by Westphal et al. (1988). Wet scavenging is applied when the rain intensity exceeds  $0.1 \text{ mm h}^{-1}$ , and the behavior of the wet dust is predicted by another prognostic equation including terms that represent advection, subgrid mixing, fallout, production due to wet scavenging, and depletion due to evaporation of rain water. We allowed evaporation of rain and its resultant re-production of dust, because it was demonstrated in the simple one-dimensional computations of Takemi (1999a) that a significant amount of rain evaporates below the cloud base owing to the very dry, deep boundary layer.

The turbulent mixing coefficient for the mixing term  $F_{mix}$  is assumed to be the same with that of other scalar variables calculated by the ARPS subgrid-turbulence parameterization.

## 2.2 Experimental design

In order to produce a squall line in the preliminary run, we placed at around the lower center of the computational domain a  $y$ -oriented line thermal having a maximum potential temperature excess of  $3 \text{ K}$  with small random perturbations added (similar to Rotunno et al. 1988).

The base-state vertical profiles of temperature, moisture, and horizontal wind are determined from the observations on 5 May 1993. The top of the mixed boundary layer is set at  $3600 \text{ m}$ , with the moisture content in the mixed layer linearly decreasing with height. The base-state horizontal winds have only the  $x$  component to simplify the experimental setups as much as possible.

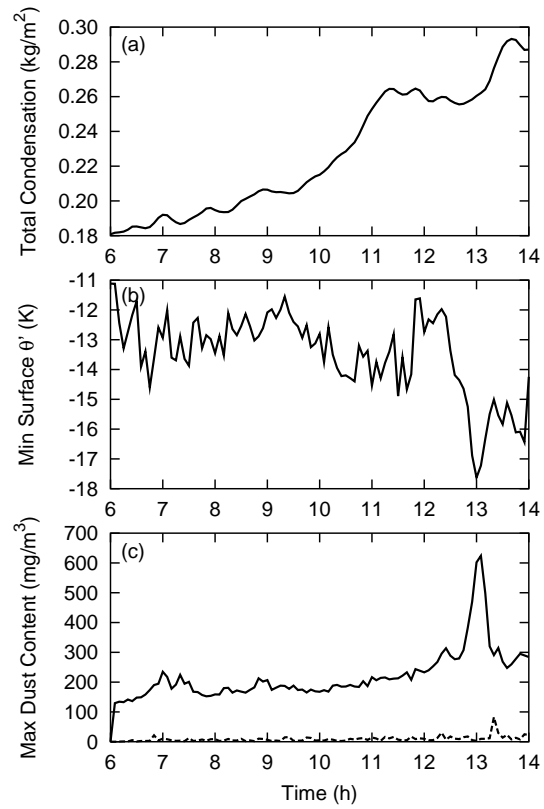


Figure 1: Temporal variations of (a) area-mean total condensation amount (i.e., water and ice content), (b) minimum surface potential temperature perturbation, and (c) domain-maximum dust concentration (solid) and rain-wet dust concentration (dashed) during 6 to 14 h. The dust particle radius in this case is  $1 \mu\text{m}$ .

With these setups the cloud model without the dust model calculations was integrated up to 6 h, and initialized with the disturbance developed at 6h the subsequent cloud development and dust emission/transport processes were simulated.

## 3. RESULTS

Overall evolutions of the simulated squall line and the associated dust transport are demonstrated in Fig. 1 for the case with the dust particle radius of  $1 \mu\text{m}$ . The maximum dust concentration varies around  $150\text{--}240 \text{ mg m}^{-3}$  after 7 h up to 12 h, while the maximum concentration of rain-wet dust is at most  $17 \text{ mg m}^{-3}$ , less than 10 % of the transported dust content. A significantly strong cold pool develops at around 13 h (Fig. 1b); this cold pool induces severer surface winds, which results in a larger amount of surface emission of dust and a maximum dust content of  $624 \text{ mg m}^{-3}$  (Fig. 1c).

The evolution of the dust transport during the squall-line development is demonstrated in Fig. 2 for the case of the  $1\text{-}\mu\text{m}$  dust radius. The areas of high dust concentration of greater than  $10 \text{ mg m}^{-3}$  are seen within the

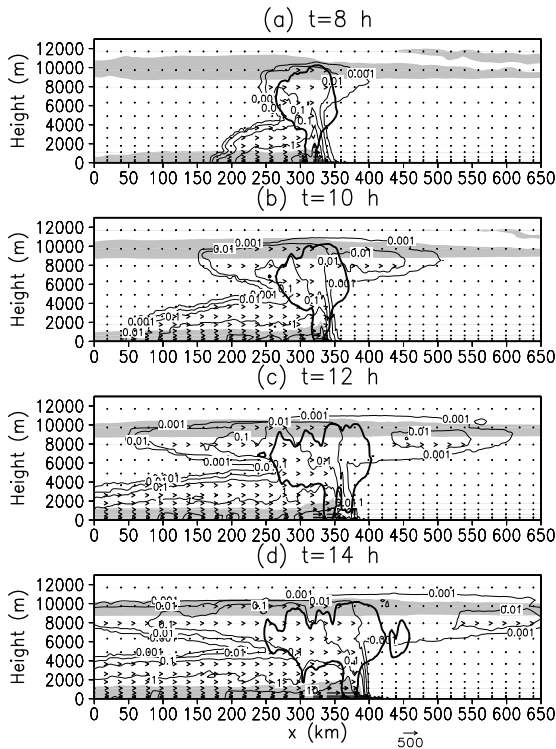


Figure 2: Line-averaged vertical cross section of dust concentration (contoured at 0.001, 0.01, 0.1, 1, and 10 mg m<sup>-3</sup>), cloud boundary (a thick, solid contour, total condensation mixing ratio of 0.1 g kg<sup>-1</sup>), potential temperature (shaded, less than -2 K), mass flux of dust (vectors, the unit of 500 mg m<sup>-2</sup> s<sup>-1</sup> shown in the lower right) (a) at 8 h, (b) at 10 h, (c) at 12 h, and (d) at 14 h for the case with the dust radius of 1 μm. The width shown corresponds to the whole computational x-domain.

surface cold pools where a large amount of the surface dust flux is induced. The areas of moderate dust concentration of more than 0.1 mg m<sup>-3</sup> are seen mainly in two areas: one is the lowest 4-km layer behind the gust front, extending rearward with time; and the second is the upper levels within and rearward of the cloud regions. This second area is at first suppressed below the 6-km level, and then penetrates into the upper layer and spreads rearward of the system in the later stages at 10, 12, and 14 h. This transport feature seems to be closely related to the system-scale (or mesoscale) circulation within a squall-line system, namely front-to-rear flow at middle to upper levels (e.g., Houze et al. 1989). The area of dust concentration of greater than 0.001 mg m<sup>-3</sup> in the upper layer gradually spreads both forward and rearward of the active convective center.

Figure 3 shows the fields of the horizontal and vertical mass fluxes of dust at the surface and vertically averaged in layers of 0–1 km, 1–3 km, 3–6 km, and 6–10 km at 10 h. The gust-front location averaged along the squall line

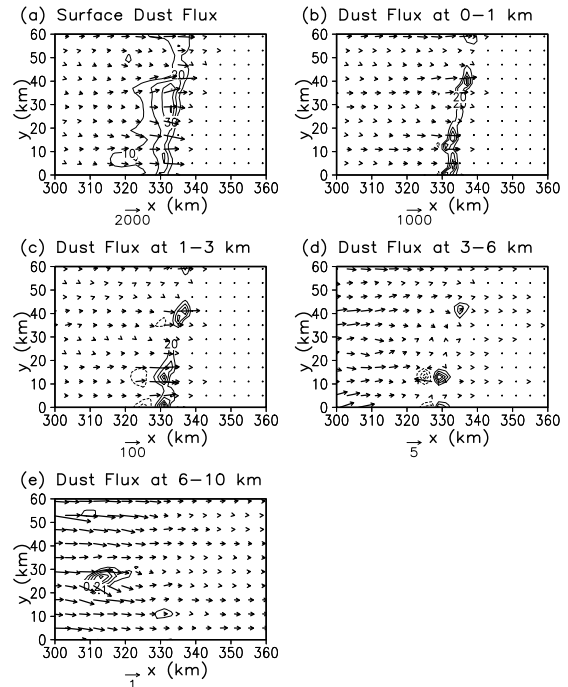


Figure 3: Horizontal cross section of horizontal dust flux (vectors), and vertical dust flux (contoured) (a) at the surface, and vertically averaged in (b) the 0–1 km layer, (c) the 1–3 km, (d) the 3–6 km, and (e) the 6–10 km at 10 h for the case with the dust radius of 1 μm. The unit vectors (in mg m<sup>-2</sup> s<sup>-1</sup>) are shown in the bottom of each panel, and the contour intervals are 10 mg m<sup>-2</sup> s<sup>-1</sup> in the panel (a), 20 in (b) and (c), 3 in (d), and 0.1 in (e).

at this time is at 334 km. A large amount of the horizontal and vertical fluxes at the surface is seen just behind the gust front and extending rearward about 10–20 km. The area of high dust flux below the 3-km level appears to be concentrated at around the gust front. The largest vertical flux in the 0–1 km layer reaches up to 80 mg m<sup>-2</sup> s<sup>-1</sup>, which is about two times larger than that at the surface, and furthermore, the peak vertical flux in the 1–3 km layer is still larger than that at the surface. This implies that the dust emitted at the surface in the cold-pool region is advected by high winds and converges at the leading edge of the cold pool to produce a large vertical flux in the boundary layer. Above the 3-km level, the area of large vertical flux has a cellular feature, and the area of larger horizontal flux is found in the rear part of the convective system.

Along the line of active transport of dust found in Fig. 3, a y-z cross section is demonstrated in Fig. 4. In the lowest 2 km there are a couple of high dust concentration areas with the horizontal spacing of about 20 km and are a large variability in the y components of fluxes (Fig. 3a). These high concentration areas seem to be extend-

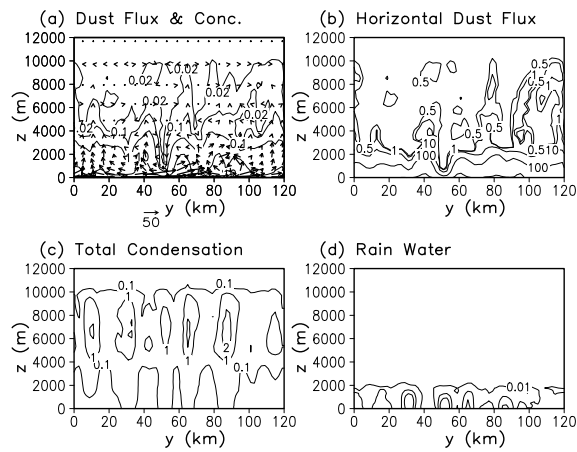


Figure 4:  $y$ - $z$  cross section (averaged between  $x = 330$  km and  $340$  km) of (a) dust flux in the  $y$ - $z$  plane (vectors, with the unit in  $\text{mg m}^{-2} \text{s}^{-1}$  shown in the bottom) and dust concentration (contoured at 0.02, 0.1, 1, and  $10 \text{ mg m}^{-3}$ ), (b) dust flux in the  $x$  direction (contoured at 0.5, 1, 10, 100, and  $1000 \text{ mg m}^{-3}$ ), (c) total condensation mixing ratio (contoured at 0.1, 1.0, and  $2.0 \text{ g kg}^{-1}$ ), and (d) rain water mixing ratio (contoured at 0.01, 0.1, and  $0.2 \text{ g kg}^{-1}$ ) at 10 h for the  $1\text{-}\mu\text{m}$ -dust case.

ing upward and then to be advected in the  $x$  direction (Fig. 3b). In Figs. 4c and 4d cloud and rain features are depicted. Above the low-level regions of high dust concentration, well-developed cloud cells and rain cells are not seen (e.g., see the column at  $y = 40$  km); namely, dust is more actively transported upward in more cloud-free and/or rain-free areas.

At the location of  $y = 40$  km in Fig. 3 upward penetration of high dust concentration as well as large dust flux is clearly seen. Thus the time lapse of wind fields as well as cloud and dust development near the gust front is closely examined at this section and is shown in Fig. 5. Initially a strong updraft is seen at the gust front at 10 h 0 min; then the strong updraft region gradually extends upward at 10 h 5 min and 10 min; and a cloud cell simultaneously develops. This type of cellular evolution is quite similar to that identified for a mid-latitude squall line (Rotunno et al. 1988); in that case periodic cellular evolution controls the multi-cellular and long-lasting behavior of a squall-line system. In the present case, the cellular evolution seems to contribute to the upward and rearward spread in the area of high dust concentration. Convective cells are regenerated at the leading edge of the cold pool during the development and evolution of the squall-line system, and therefore, the cycle of the dust transport shown in Fig. 5 continuously takes place along the squall line. This regeneration of convective cells and the associated cycle of dust transport determines the system-scale feature of the dust transport demonstrated in Fig. 2.

In Fig. 5 the highest concentration of dust is seen within the cold pool; the concentration contour of  $10 \text{ mg m}^{-3}$

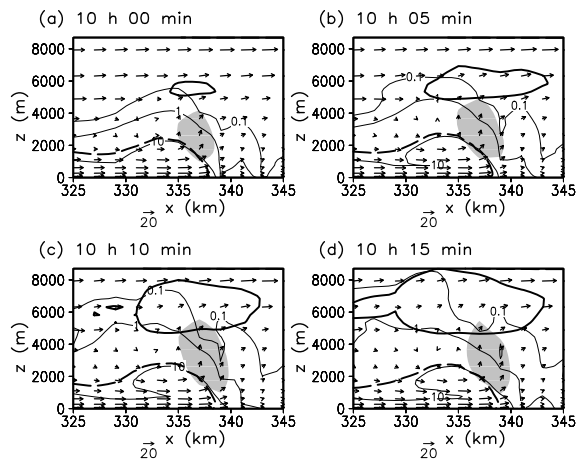


Figure 5:  $x$ - $z$  cross section (averaged between  $y = 35$  km and  $45$  km) of dust concentration (contoured at 0.1, 1.0, and  $10 \text{ mg m}^{-3}$ ), potential temperature perturbation ( $-2 \text{ K}$  contour with a thick, dashed line), total condensation mixing ratio ( $1.0 \text{ g kg}^{-1}$  contour with a thick, solid line), strong updraft region (shaded), vertical velocity of greater than  $6 \text{ m s}^{-1}$ , and wind vector (in  $\text{m s}^{-1}$ , the unit shown in the bottom of each panel) (a) at 10 h, (b) at 10 h 5 min, (c) at 10 h 10 min, and (d) at 10 h 15 min.

$\text{m}^{-3}$  is nearly identical with the cold-pool boundary. Dust emitted by cold-pool-induced high winds at the surface seems to be at first mixed within the cold pool, which can be regarded as a reservoir of dust. In this situation, the transfer of dust through the interface of cold pool will be crucial for the upward transport of dust by convective updrafts. In order to examine the mixing characteristics around the cold-pool boundary, the turbulence fields from the subgrid-mixing parameterization were examined (not shown). It was clearly indicated that the turbulence intensity and the eddy viscosity coefficient are larger at and around the leading edge of the cold pool than within and ahead of the cold pool. This feature strongly suggests that active turbulent mixing at the leading edge of the cold pool plays a key role in transferring dust reserved in the cold pool out to updraft region and upper into the upper atmosphere. In other words, cold pool dynamics, causing high friction velocity to induce dust emission, mixing and transferring dust through the leading edge, and generating vigorous updrafts to raise dust, largely controls the behavior and evolution of dust transport from the surface to the upper layer.

In the foregoing we have argued the importance of the dynamical effects by cold pool on dust transport. We will here assess the amount of transported dust in various domains relative to the gust front position. Considering the dust transport feature shown in Fig. 2, we divide the whole computational domain into the following: DOMAIN1, the 0–1 km layer behind the gust front; DOMAIN2, the 1–5 km layer behind the gust front; DOMAIN3, the 5–10 km layer behind the gust front; and DO-

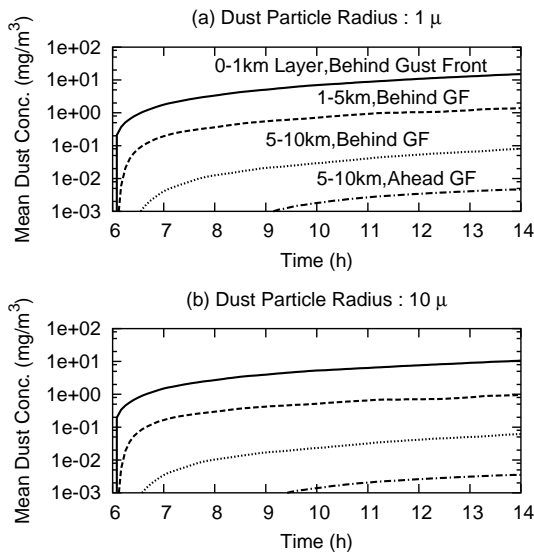


Figure 6: Temporal variations of domain-averaged dust concentration (in  $\text{g m}^{-3}$ ) for the cases with the dust particle radius of (a)  $1 \mu\text{m}$  and (b)  $10 \mu\text{m}$ . See the text for the details of the domains defined here.

MAIN4, the 5–10 km layer ahead of the gust front. Figure 6 shows the temporal variation of the mean dust concentration in each defined domain for the cases with the dust radius of  $1 \mu\text{m}$  and  $10 \mu\text{m}$ . The dust concentrations in all domains steadily increase as the dust is continuously supplied from the ground. The mean concentration diminishes by an order of magnitude as the domain goes from DOMAIN1 to DOMAIN2, DOMAIN3, and further to DOMAIN4. Within the cold pool region (DOMAIN1) the concentrations for the  $1\text{-}\mu\text{m}$  and  $10\text{-}\mu\text{m}$  cases reach as high as  $18.6 \text{ mg m}^{-3}$  and  $13.3 \text{ mg m}^{-3}$  respectively at 14 h. Behind the gust front, the mean concentration in the 1–5 km levels are still above  $1 \text{ mg m}^{-3}$ . There is a significant difference between the dust concentrations ahead of and behind the gust front in the upper layer of 5–10 km:  $144 \mu\text{m m}^{-3}$  in DOMAIN3; and  $4 \mu\text{m m}^{-3}$  in DOMAIN4.

In this way, the amount of transported dust significantly differs not only in the boundary layer but also in the upper atmosphere depending on the region relative to the gust front, and thus seems to be significantly controlled by the dynamical effects of the surface cold pool. This behavior can again be interpreted by the reasoning of Rotunno et al. (1988); as the cold pool intensifies, the updraft is then tilted rearward and hence the front-to-rear flow prevails at middle to upper levels from a system-scale viewpoint, which will result in more active transport of dust in the upper-rear part of the system.

#### 4. SUMMARY AND CONCLUSIONS

Three-dimensional cloud-resolving simulations (with the horizontal resolution of 2 km) coupled with a dust

emission/transport model were performed in order to explicitly represent convective- and cloud-scale processes such as updraft/downdraft, surface cold pool, precipitation, and cloud microphysics and thereby to investigate the effects of these convective processes on dust emission and transport from a cloud-scale to a mesoscale perspective. The case of the 5 May 1993 duststorm over the Gobi Desert, which was caused by a squall-line-type mesoscale convective system (Takemi 1999b), was examined in this study, and the model was set up in an idealized fashion to better concentrate on the primary mechanisms for convective-scale dust transport within a squall-line-type convective system. In modeling the dust emission and transport processes we followed a standard approach from the previous dust modeling studies. Owing to the computer resources available and in addition to some uncertainties which may obscure the central focus of this study, we assumed the dust particle as a single-sized one. Although the simulations are configured in the idealized settings, the maximum dust concentration reached as high as  $624 \text{ mg m}^{-3}$  which is in fair agreement with the reported value during the observed event ( $1016 \text{ mg m}^{-3}$ , Mitsuta et al. 1995); this makes the results and analyses of the present idealized simulations more reasonable.

Dust, once emitted at the surface, is transported upward in the lower atmosphere by convective-scale updraft which is forced continuously at the leading edge of the squall-line cold pool and then spreads in the cross-line directions in a layered fashion at upper levels by system-scale circulation. In the upper layer the rearward transport of dust is more pronounced than the forward transport, owing mainly to the front-to-rear flow which can be typically found in the squall-line convective systems.

The surface winds are the strongest within the cold-pool region, and as a result a high dust concentration is found and mixed within the cold pool. In other words, cold pool can be regarded as a reservoir of dust. In order for the dust contained in the cold pool to be entrained in the convective updraft, the mechanisms for the transfer of the contained dust out of the cold pool will then be crucial. The analysis of the subgrid-turbulence characteristics at and around the cold-pool boundary indicates that the turbulent mixing at the leading edge of the cold pool plays a key role in transferring dust out of the cold pool. After transferred into the updraft region out of the cold pool, dust will be transported into the upper atmosphere. This process of the convective-scale dust transport continuously occurs along the leading edge of the cold pool through the regeneration of convective cells along the line during the convective-system evolution.

The amount of the transported dust from a system-scale perspective significantly depends on the domain relative to the location of the gust front. The upper-level mean dust concentration is by more than an order of magnitude larger in the rear part of the system than in the forward part of the system.

It is concluded that the turbulent mixing and forced up-draft at the leading edge of the squall-line cold pool and the intensity of the cold pool itself primarily determine and control the convective-scale as well as system-scale characteristics of dust transport.

The present study has dealt specifically with the squall-line case. The same argument presented here can also be applied to dust transport processes associated with synoptic-scale cold-frontal rainbands, since they show a similar structure with the squall-line system: namely, linear convective structure; deep convection development along the rainband; and a significant temperature gradient (frontal structure) at the surface. These elements may act cooperatively with each other in transporting dust from a convective-scale perspective. Therefore, it is suggested that the representations of convective-scale vertical transport processes should be adequately updated in order to improve the accuracy of the regional- to global-scale numerical predictions with grid spacings insufficient to resolve convective motions.

This study employed a horizontal grid spacing of 2 km, which is assumed to be sufficient for cloud-resolving simulations, and revealed the basic mechanisms for convective dust transport. However, there are a number of issues to be resolved in a future work. For example, we stressed the importance of turbulent mixing at the interface of the cold pool and the pre-front environment. As can be seen in many dust front pictures (e.g., Fig. 2 of Mitsuta et al. 1995), the frontal surface indicates a highly turbulent structure. In order to quantitatively evaluate the amount of dust transfer, a very-high-resolution simulation that is capable of representing more detailed structures of the cold-pool edge may be required. In addition, we assumed in this study that the subgrid-turbulent mixing coefficient for dust content is the same with that for other scalar variables such as potential temperature and moisture content. The issue of the subgrid mixing parameterization for dust content should also be tackled in the near future.

## 5. ACKNOWLEDGMENT

This research was supported by the Special Coordination Fund for Promoting Science and Technology from the Ministry of Education (MEXT) of Japan. The ARPS model was developed by the Center for Analysis and Prediction of Storms (CAPS), The University of Oklahoma. CAPS is supported by the National Science Foundation and the Federal Aviation Administration through combined grant ATM92-20009.

## 6. REFERENCES

Businger, J. A., J. C. Wyngaard, Y. Izumi, and E. F. Bradley, 1971: Flux-profile relationships in the atmospheric surface layer. *J. Atmos. Sci.*, **28**, 181–189.

Houze, R. A., Jr., S. A. Rutledge, M. I. Biggerstaff, and B. F. Smull, 1989: Interpretation of doppler weather radar

displays of midlatitude mesoscale convective system. *Bull. Amer. Meteor. Soc.*, **70**, 608–619.

Liu, M., and D. L. Westphal, 2001: A study of the sensitivity of simulated mineral dust production to model resolution. *J. Geophys. Res.*, **106**, 18099–18112.

Mitsuta, Y., T. Hayashi, T. Takemi, Y. Hu, J. Wang, and M. Chen, 1995: Two severe local storms as observed in the arid area of northwest China. *J. Meteor. Soc. Japan*, **73**, 1269–1284.

Parungo, F., Z. Li, X. Li, D. Yang, and J. Harris, 1994: Gobi dust storms and The Great Green Wall. *Geophys. Res. Lett.*, **21**, 999–1001.

Qian, W., L. Quan, and S. Shi, 2002: Variations of the dust storm in China and its climatic control. *J. Climate*, **15**, 1216–1229.

Rotunno, R., J. B. Klemp, and M. L. Weisman, 1988: A theory for strong, long-lived squall lines. *J. Atmos. Sci.*, **45**, 463–485.

Shao, Y., E. Jung, and L. M. Leslie, 2002: Numerical prediction of northeast Asian dust storms using an integrated wind erosion modeling system. *J. Geophys. Res.*, **107**, 4814, doi:10.1029/2001JD001493.

Takemi, T., 1999a: Evaporation of rain falling below a cloud base through a deep dry atmospheric boundary layer over an arid region. *J. Meteor. Soc. Japan*, **77**, 387–397.

Takemi, T., 1999b: Structure and evolution of a severe squall line over the arid region in northwest China. *Mon. Wea. Rev.*, **127**, 1301–1309.

Takemi, T., and T. Satomura, 2000: Numerical experiments on the mechanisms for the development and maintenance of long-lived squall lines in dry environments. *J. Atmos. Sci.*, **57**, 1718–1740.

Takemi, T., and N. Seino, 2004a: Duststorms and cyclone tracks over the arid regions in East Asia in spring. *J. Geophys. Res.*, in press.

Takemi, T., and N. Seino, 2004b: Duststorms and mesoscale cloud systems over the East Asian Deserts in spring. *Water, Air, & Soil Pollution*, revised.

Uno, I., G. R. Carmichael, D. G. Streets, Y. Tang, J. J. Yienger, S. Satake, Z. Wang, J. -H. Woo, S. Guttikunda, M. Uematsu, K. Matsumoto, H. Tanimoto, K. Yoshioka, and T. Iida, 2003: Regional chemical weather forecasting system CFORS: Model descriptions and analysis of surface observations at Japanese island stations during the ACE-Asia experiment. *J. Geophys. Res.*, **108**, 8668, doi:10.1029/2002JD002845.

Westphal, D. L., O. B. Toon, and T. N. Carlson, 1988: A case study of mobilization and transport of Saharan dust. *J. Atmos. Sci.*, **45**, 2145–2175.

Xue, M., K. K. Droegemeier, and V. Wong, 2000: The Advanced Regional Prediction System (ARPS) - A multi-scale nonhydrostatic atmospheric simulation and prediction tool. Part I: Model dynamics and verification. *Meteor. Atmos. Physics*, **75**, 161–193.